CLM-R 28

CLM-R 28

United Kingdom Atomic Energy Authority

RESEARCH GROUP

Report

STABILIZED PINCH EXPERIMENT

H. S. COCKROFT
A. MALEIN
P. A. SHATFORD

Culham Laboratory,

Culham, Abingdon, Berks.

1963

Available from H.M. Stationery Office
FOUR SHILLINGS NET

U.D.C.
533.952
621.039.627

STABILIZED PINCH EXPERIMENT

by

H.S. Cockroft
A. Malein
P.A. Shatford

A B S T R A C T

Experiments on a long linear pinched discharge are described. Under all conditions the current skin separating the axial and azimuthal magnetic fields is found to be relatively diffuse. The observed instability growth rates correspond more closely to the theoretical values for a fully diffuse pinch than to those for a sharp ('stabilized') pinch. The rate of diffusion of magnetic field is the greater the lower the initial filling pressure, a result qualitatively in agreement with the measurements on Zeta in the so-called 'anomalous resistivity' regime.

U.K.A.E.A. Research Group,
Culham Laboratory,
Nr. Abingdon,
BERKS.

September, 1962.
(C/18)ED

C O N T E N T S

Introduction

1. The possibility of completely stabilising a pinched discharge by the combination of a trapped axial magnetic field (for the short wavelength perturbations) and a surrounding conducting wall (for the longer wavelengths) has been discussed by many authors. Relatively simple stability criteria are obtained if it is assumed that the pinch currents flow only on the plasma surface[1-3]. Permitting the current sheath to have a small but finite thickness leads to more complex criteria[4,5]. In particular it is then necessary for stability that there should be a small axial magnetic field external to the pinch opposite in direction to the trapped internal field. The necessary and sufficient conditions for the stability of a diffuse pinch, that is, one with a thick current sheath, have been derived by Newcomb [6]. These conditions cannot readily be applied to measured field distributions since considerable numerical analysis is needed for each case. Suydam[7] has given a simple necessary condition for the stability of such pinches which is relatively easy to use.

2. The theoretical work mentioned above treats the plasma as an inviscid fluid of infinite conductivity. It has been extended to include the effects of finite conductivity[8] and anisotropic pressure[9,10] both of which can give new instabilities. Other instabilities have been predicted in current carrying plasmas due to the interaction of plasma waves with those particles which have a velocity slightly greater than the phase velocity of the wave[11].

3. The final effect of the different forms of instability depends on large amplitude behaviour which cannot be treated by the linear theory used to predict the instabilities. Thus experimental investigations are required to confirm the theoretical models and to discover what happens when large amplitudes develop.

4. Experimentally a field configuration which completely satisfied the theoretical conditions for hydromagnetic stability of a pinched discharge has never been produced and a completely stable pinch has never been observed. Experiments with the hard core configuration have shown instability when the criteria for hydromagnetic stability (with an infinite conductivity perfect fluid) were well satisfied[12,13].

5. In the pinch experiments to be described no attempt was made to satisfy all the hydromagnetic stability requirements; for example, the axial field external to the plasma was not reversed. Thus the results concern the formative stage of the discharge and we also seek to know whether the later instability of the system is or is not consistent with

hydromagnetic theory.

The Apparatus

6. The discharge tube, shown schematically in Fig. 1 was 3.25 m long and 30 cms bore. Earlier work with shorter tubes had shown that such a length was necessary to obtain a length of plasma column with properties independent of axial position. The main capacitor bank, storing 40 kJ at 25 kV, was connected to the discharge tube through fourteen four-electrode spark gaps working in parallel. The total external inductance was of order 50 mμ H. The initial axial field was produced by an auxiliary condenser bank and was variable up to 3 kG with a rise time of 58 msecs.

7. Preionisation was not used. With hydrogen as the filling gas the tube would not break down at pressures below 20 μ (line density $N = 10^{18}$/cm). With helium filling this threshold was 40 μ and with argon 3 μ.

8. The total energy input per ion (p = 20 μ $Hg_{,}$ V = 25 kV) was 830 eV from the main bank and 95 eV from the Bz bank (Bo = 2000 G). During the first half cycle, lasting 27 μsecs, the total energy dissipated was about 30 kJ corresponding to 600 eV/ion and a mean resistance of 30 mΩ. At peak current the resistance was 20 mΩ. At 5 μsecs the total energy input from the main bank was 15 kJ and assuming constant resistance (30 mΩ) 3 kJ (= 60 eV/ion pair) had been dissipated.

9. Streak photographs were taken through quartz windows, one near the middle of the tube 1.7 m from the cathode end, the other 0.85 m from the cathode end. Magnetic field measurements were made in a quartz probe tube 13 mm O/D which could be placed across the tube at the centre window.

Current and Voltage Waveforms

10. Fig.2 shows typical voltage and current waveforms. The voltage measurement included most of the external inductance (electrodes and cable collector plate) and there is therefore negligible recorded voltage drop when the tube is fired. With the highest rate of rise of current the voltage drop in the external inductance is less than 3 kV.

11. The shape of the current pulse depends on the initial axial magnetic field and on gas pressure. As these increase the discharge is held close to the wall for a longer time and the initial rate of rise of current increases.

12. At the higher pressures a small amplitude oscillation occurs on the current trace due

to inertia of the plasma. It also appears on the magnetic probe signals, particularly Bz near the tube centre, and a corresponding fluctuation in radius can be seen on the streak pictures. Frequencies observed are between 150 kc/sec and 1 Mc/sec. The low frequencies are obscured by onset of instability and the high ones are of small amplitude as expected from consideration of the rate of collapse of the discharge. The period of oscillation can be used to estimate the mass of gas involved[14] according to the following theory.

13. If the mass of gas is assumed to be concentrated at the current sheath at radius r, then the outward force per unit length on the gas is

$$F = \frac{\pi r}{\mu}\left(B_i^2 - B_e^2 - B_\theta^2\right) = \frac{1}{\pi\mu}\left(\frac{\phi_i^2}{r^2} - \frac{\phi_e^2 r}{(a^2-r^2)^2} - \frac{\mu^2 I^2}{4r}\right) \qquad (1)$$

with

B_i	the internal longitudinal magnetic field
B_e	the external longitudinal magnetic field
B_θ	the azimuthal magnetic field at radius r
ϕ_i	the internal longitudinal flux
ϕ_e	the external longitudinal flux
a	the radius of the outer conducting shell
I	the total current
μ	the permeability of free space.

The units are M.K.S.

In equilibrium F = 0 and for small displacements x from equilibrium the force will be $x\frac{\partial F}{\partial r}$. During these displacements ϕ_i and ϕ_e remain constant but I changes by an amount i. The acceleration is then

$$\ddot{x} = \frac{x}{m}\frac{\partial F}{\partial r} = \frac{x}{\pi\mu m}\left[-\frac{3\phi_i^2}{r^4} - \phi_e^2\frac{(a^2+3r^2)}{a^2-r^2} + \frac{\mu^2 I^2}{4r^2} - \frac{\mu^2 I}{2r}\cdot\frac{i}{x}\right] \qquad (2)$$

14. To determine $\frac{i}{x}$ we assume the source to be a voltage Vo with a series impedance Z, then the voltage across the tube (V) is given by

$$V = V_o - IZ = \frac{\partial\phi\theta}{\partial t} = \frac{\mu l}{2\pi}\left(\dot{I}\log\frac{a}{r} - I\frac{\dot{r}}{r}\right) \qquad (3)$$

where l is the tube length. Now treating I, r and Vo as constant with a superimposed oscillation at frequency ω of amplitude i and x on I and r respectively we get

$$\frac{i}{x} = j\frac{\omega I}{r}\cdot\frac{\mu l}{2\pi}\left[Z + j\omega\cdot\frac{\mu l}{2\pi}\log\frac{a}{r}\right]^{-1} \qquad (4)$$

Substituting equation (4) in equation (2), using equation (1) with F = 0 and substituting for ϕ in terms of B, the following equation for ω can be obtained.

$$\omega^2 = \frac{\mu I^2}{2\pi m r^2}\left[1 + \frac{1}{\log\frac{a}{r}\,1 + \frac{Z}{j\omega\frac{\mu l}{2\pi}\log\frac{a}{r}}} + \frac{2a^2}{(a^2 - r^2)}\frac{B_e^2}{(B_i^2 - B_e^2}\right] \qquad (5)$$

In our case the external impedance Z is small compared with the tube impedance $j\omega\frac{\mu l}{2}\log\frac{a}{r}$, and the last term is usually negligible. The formula then reduces to

$$\omega^2 = \frac{\mu I^2}{2\pi m r^2}\left[1 + \frac{1}{\log\frac{a}{r}}\right]$$

or

$$m = 5 \times 10^{-9}\left(\frac{I}{rf}\right)^2\left(1 + \frac{1}{\log\frac{a}{r}}\right) \text{ kg/metre}$$

with I in amps, r in metres and f in cycles/second. The oscillation period and values of m are given in Table I. If the plasma is assumed to be uniformly distributed inside the current sheath and $\dot{r}$ and $\ddot{r}$ proportional to r, then the value of m is multiplied by 1.5.

15. When the tube has been conditioned for some time values of m are between $\frac{1}{3}$ and $\frac{3}{4}$ of the mass of gas initially in the tube calculated from the initial pressure. The variation is not related to initial pressure or field and is probably due to differences in tube condition. The effect has not been investigated systematically but higher values of m are obtained after the tube has been up to atmospheric pressure. Since the frequency changes during collapse there is some difficulty in selecting the appropriate I, f, and r, and great accuracy cannot be obtained.

16. The 'resistance' of the discharge at maximum current (applied voltage/current) is recorded in Table I together with a temperature obtained by assuming a uniform conductivity σ over the current channel and $\sigma = 19.2\ T^{3/2}$ mho/cm (15). The radius was taken to be $r_m = 800\ Bo/I$ with Bo the initial magnetic field in gauss and I the peak current in amps giving r in cms as tabulated. This formula corresponds to a uniform longitudinal current density and half the total B_z flux inside a radius r_m with pressure balance between magnetic fields. The discharge is usually unstable before maximum current is reached, the current distribution is therefore not known and a significant conductivity from which to deduce temperature cannot be determined. Also probe measurements show that at peak current the flux is still increasing due to motion of the plasma and the voltage is therefore partly inductive.

<u>TABLE I</u>

<u>INITIAL VOLTAGE 18 kV</u>

Initial Conditions				Radial Oscillations		At Maximum Current				Diffusion	
Initial Field Gauss	Gas Pressure Microns Hg		Mass kg/m x10^{-6}	Period μ secs	Mass m kg/m x 10^{-6}	Current K.A.	Resistance mΩ	Radius cms	Temperature eV	Time Tu μsecs	$\int \omega_m dt$
360	H_2	22	1.8	-		110	64	2.6	5.0	4	6.8
	H_2	42	3.5	2.0	2.85	110	82	2.6	4.2	4	8.0
720	H_2	22	1.8	-		135	38	4.3	3.6	4	7.1
	H_2	42	3.5	2.0	1.7	140	32	4.1	4.2	6	5.7
	H_2	110	9.1	4.0	7.0	142	28	4.1	4.8	11	5.4
	H_2	200	16.5	5.0	12.6	138	27	4.2	4.6	12	3.4-5.4
	He	38	6.3	2.2	2.66	148	22	3.9	6.0	11	6.0
	He	84	13.9	3.6	6.1	145	14	4.0	7.8	11	4.7-6.7
	A	4	6.6	3.0	5.0						4.2
1440	H_2	22	1.8	-		170	18	6.8	3.2	7	5.4
	H_2	42	3.5	-		173	11	6.7	4.6	10.5	4.3
	H_2	120	10.0	-		166	13	6.9	4.0	16	2.7
	H_2	200	16.5	-		170	14	6.8	3.8	16	2.2
	He	84	13.9	3.0	5.4	172	7	6.7	7.2	16	4.7-5.4

<u>INITIAL VOLTAGE 25 kV</u>

Initial Field Gauss	Gas	Pressure Microns Hg	Mass kg/m x10^{-6}	Period μ secs	Mass m kg/m x 10^{-6}	Current K.A.	Resistance mΩ	Radius cms	Temperature eV	Time Tu μsecs	$\int \omega_m dt$
360	H_2	22	1.8	-		169	57	1.7	9.4	3	6.0
	H_2	40	3.3	1.2	1.0					5	6.7
720	H_2	22	1.8	-						7	6.6
	H_2	44	3.6	1.2	1.2	177	62	3.3	3.8	7	8.6
	H_2	200								11	
1440	H_2	22	1.8	-		213	26	5.4	3.4	10	5.2
	H_2	44	3.6	1.5	1.6	220	32	5.2	3.2	11	5.3
2160	H_2	22	1.8	-		234	26	7.4	2.2	9	4.4
	H_2	44	3.6	-		241	27	7.2	2.2	10	3.9
	H_2	600	50	-		248	-	7.0		16	1-2.4

Magnetic Field Measurements

17. The magnetic field distribution was measured by probe coils in a 13 mm O/D quartz tube. The coils were 2 cm apart and could be oriented to measure either B_θ or B_z. The streak picture at the window with the probe tube showed earlier disintegration of the luminous channel when the probe was in position. The probe results are therefore not reliable.

18. Plots of field vs radius (Fig.3) showed always a slower collapse rate on the free end side of the probe and so a current channel which moved up to 2 cm off centre with high initial fields and 5 cms off centre with low initial fields. This was followed by a movement around the axis which started at 8 μ secs and completed half a revolution in 2-3 μ secs. These times increased slowly with pressure and initial magnetic field. Small variations in the rate of movement off centre and in the time at which rotation started account for most of the irreproducibility of the probe signals.

19. Breakdown appeared to occur always near the wall of the tube and an initially thin (2-3 cm) current sheath moved towards the centre. The rate at which this diffused decreased as pressure and initial magnetic field increased. Thus the temperature appears to depend more on how long the gas is held near the wall than on the amount of gas to be heated. The time t_u at which diffusion resulted in maximum longitudinal current density near the axis is shown in Table I. If we assume t_u is given by $t_u = \frac{1}{4}\sigma\mu r^2$ and the conductivity σ by [15] $\sigma = 19.2\ T^{3/2}$ then $T\ (eV) = \left[\frac{16.5\ t_u\ (\mu\ secs)}{r^2\ (cms)}\right]^{2/3}$. Using a mean value of r this gives Te ~ 2 eV for the high voltage results and 1-2 eV for the low voltage ones. The times of 16 μsecs with helium and 600 μH_2 give ~ 3 eV. The formula for t_u is taken from Adlam and Tayler[16] and is the time for an initial surface current to diffuse to a sensibly uniform current in a conductor radius r and conductivity σ. In that case uniform current is an equilibrium distribution. In our case the conductor is free to move and there is not equilibrium but current density near the axis continuously increases. This case has not been treated theoretically but the time to uniform current will be of the same order of magnitude as in the case of simple diffusion in a rigid conductor. (Plasma pressure and inertia and instabilities are being neglected.)

20. The dependence of diffusion rate on pressure was not appreciated until the experimental work had ended and there are therefore few results at pressures high enough to give a good tubular pinch. In general the pressure was kept low expecting that this would produce a higher temperature and thus a better tubular pinch, and also keep the

growth rate of instabilities high so that they would be observed before the current had decreased appreciably.

21. The radius of the discharge deduced from probe measurements was in general about one centimetre larger than the radius measured to the outside of the luminous channel on streak pictures taken at the window without the probe.

Light Output

22. A monochromator fitted with a photomultiplier was used under one set of conditions viz. main bank voltage 18 kV, Bo 720 gauss. With the original continuous flow gas system (time constant ~ 30 secs) the intensity of CIII λ 2297Å impurity light was found to depend on the time interval between shots. With minimum interval (about 20 secs) the signals from CIII and Hα were of about the same amplitude. With long intervals CIII light was small during the first 8 μsecs. The gas system was changed, the tube being pumped out with the diffusion pump between shots and filled a few seconds before firing. The intensity of CIII fell to less than 1/500 of Hβ intensity during the first 10 μsecs. The streak picture was not affected. Hα and Hβ intensities both had peaks at about $3\frac{1}{2}$ μsecs as shown in Fig.4.

Streak Photographs

23. Streak photographs were taken at two windows one at the centre of the tube (about $1\frac{1}{2}$ m from each electrode) and one 75 cms from the cathode. In general the centre window had a 13 mm diameter quartz probe tube across a diameter and this was viewed end on by the streak camera. As shown in Fig.5 the probe tube had a considerable effect on the streak picture, causing earlier instability and smaller radius than at the window with no probe. When the probe tube was removed the two pictures were similar, the one at the window without the probe tube being unaffected. As far as could be checked with this arrangement discharge diameters deduced from probe measurements and streak photographs were the same for the first few micro-seconds and it has been assumed that the outer edge of the luminous channel gives a fair measurement of the position of the current sheath. In what follows radii and times to instability were measured on pictures taken at the window without the probe tube, Fig.6 shows some of these streak pictures with different initial conditions.

24. Figs. 7(a-j) show the discharge radius measured on the streak photographs plotted against $\frac{\mu I}{2\pi a B_o}$, the ratio of azimuthal magnetic field at the outer conductor to initial (uniform) magnetic field. The plot is based on a simple model of the discharge in which

all the current is supposed to flow in a thin skin of radius r' giving a field distribution $(0,0,B_i)$ for $r < r'$ and $(0,\frac{\mu I}{2\pi r}, B_e)$ for $r > r'$. Then neglecting plasma pressure and inertia, pressure balance between the magnetic fields gives

$$\left(\frac{\mu I}{2\pi r}\right)^2 = B_\theta^2 = B_i^2 - B_e^2$$

and longitudinal flux conservation inside the conducting sheath at radius a, gives

$$\phi_o - \phi_i = B_e(a^2 - r^2)$$

where

$$\phi_o = B_o\, a^2 \text{ and } \phi_i = B_i\, r^2 .$$

Then with $R = r/a$ and $k = \phi_i/\phi_o$ we obtain the equation

$$\frac{\mu I}{2\pi a B_o} = \frac{k}{R}\left[1 - \left(\frac{\frac{1}{k} - 1}{\frac{1}{R^2} - 1}\right)^2\right]^{\frac{1}{2}}$$

In Fig.8, R has been plotted vs. $\frac{\mu I}{2\pi a B_o}$ for different values of k, and the curves with k = 1 and 0.5 have also been drawn in Fig.7 for comparison with the experimental points.

25. The experimental curves are very nearly parallel to the constant k lines or oscillate about them due to inertia of the gas, and a naive interpretation would be that, while the initial trapping of flux may be poor, containment is good until instability occurs. With hydrogen at 20 μ and 40 μ pressure $k \sim 0.5$ corresponding to the flux initially inside $r \sim 12.5$ cms. Thus we might imagine that the current sheath forms initially about 2.5 cms from the wall and the region outside the current skin remains a poor conductor for the first few microseconds. At higher pressures and with helium and argon the initial k is higher, approaching 0.73 corresponding to skin formation on the wall of the tube.

Stability of the discharge

26. The theoretical stability of a pinch discharge with currents flowing only on the plasma surface has been considered in Refs. 1-3. Tayler's formula for growth rate ω (Ref.3) with $\beta\gamma \ll 1$ (plasma pressure negligible) has been used to draw Fig.9 which shows the maximum growth rate to be expected as a function of R and $\mu I/2\pi\, aB_o$. The growth rate depends on k, the wavenumber of the instability, and the maximum value, which occurs at $k\, r_o \sim 0.5$, has been used. This maximum growth rate has been normalised to $\omega_o = \frac{B_o}{2}\left(\frac{\pi}{\mu m}\right)^{\frac{1}{2}}$ which is the reciprocal of the time for an Alfven wave to cross the tube with the initial axial field. In Fig.10 is plotted $\frac{\omega_m}{\omega_o}$, where ω_m is the reciprocal of the time for an Alfven wave to cross the discharge. ω_o is always less than ω_m. The instability considered in this treatment involves movement of the whole of the discharge ('gross' instability)

and the growth rate is a maximum at $kr \sim 0.5$.

27. When the current skin is assumed to have a finite thickness instabilities are found which do not involve plasma near the axis of the discharge[4-7]. If the field outside the discharge is in the same direction as that inside, a short wavelength instability with $2 < kr < {}^{1}/_{b_e}$ is always possible, and one with $kr \sim 5.0$ can occur up to a line shown dotted in Fig.9. The growth rate of these instabilities has been considered by Bickerton[17] who concludes that it is in general an order of magnitude less than ω_m. The model used is probably adequate for the long wavelength instability which involves the plasma where $B_\theta < B_z$ but the short wavelength instabilities involving the region where $B_z < 2B_\theta$ are on the outside of the current skin where the plasma density is probably low and the growth rate correspondingly greater.

28. These comments are based on Tayler's theory[5] as shown in Fig.11. Here δW (which is proportional to growth rate squared) has been plotted vs kr with different values of Λ and b_e ($\frac{a}{r}$ and $\frac{B_e}{B_\theta}$ respectively) and the diagram shows how as b_e increases from zero the short wavelength instabilities appear at $kr \leqslant {}^{1}/_{b_e}$ and how as Λ increases the one with $kr \sim 0.5$ appear. The line for stability at $kr \sim 0.5$ on Fig.9 corresponds to combinations of Λ and b_e which just touch the line $\delta W = 0$ in the region $Kr \sim 0.5$.

29. The diagram suggests that the short wavelength instability could be avoided by making $B_z = 0$ at the outer edge of the plasma.

30. To get an idea of the type of instability involved ω_m has been plotted vs. time for each case and the integral $\int \omega_m dt$ evaluated from $t = 0$ to the time when the discharge became obviously unstable on the streak photograph. Values of the integral are given in Table 1. If ω_m were the true growth rate we should expect (since 1% fluctuations in the fields occur from early times) to see instability when $\int \omega_m dt \sim 4$ corresponding to a fifty-fold (e^4) increase in the initial perturbation. Values of 8 ($e^8 \sim 2500$) would seem to be improbable. If surface instabilities with growth rates $\sim \omega_m/10$ are involved then the integral should reach values of ~ 40. The values found range from 2-8 and therefore seem to be quite incompatible with surface instabilities. Also the low values occur with high fields when R is large and $\omega << \omega_m$ (see Fig.9) and much higher values (> 10) would be expected even for the gross instability.

Conclusion

31. The experimental work was disappointing in that a good tubular pinch was not obtained

and consequently the growth rate of instabilities was ω_m rather than ω. The inter-diffusion of the magnetic field components B_θ and B_z was the faster the lower the initial filling pressure. This is unexpected in that qualitatively one would expect the electron temperature and therefore the conductivity to be the higher the lower the particle density. The observed behaviour is similar to that seen by Lees et al[18] in the Zeta machine.

REFERENCES

1. ROSENBLUTH, M.N. The stabilized pinch. Third International Congress on Ionization Phenomena in Gases, Venice, 1957. Proceedings, pp.903-907.

2. SHAFRANOV, V.D. On the stability of a cylindrical gaseous conductor in a magnetic field. J. Nucl. Energy, vol.5, no.1, pp.86-91, 1957. (Trans. from Atomnaya Energia, vol.1, no.5, 1956.)

3. TAYLER, R.J. The influence of an axial magnetic field on the stability of a constricted gas discharge. Proc. Phys. Soc., section B, vol.70, no.455, pp.1049-1063, November, 1957. (Based on A.E.R.E. T/R 2262.)

4. ROSENBLUTH, M.N. Stability and heating in the pinch effect. Second International Conference on the Peaceful Uses of Atomic Energy, Geneva, 1958. Proceedings, vol.31, pp.85-92. (Paper 347.)

5. TAYLER, R.J. Lectures on the hydromagnetic stability of a cylindrical plasma. Pt.3. Surface instabilities of the stabilized pinch. A.E.R.E. - L 104. 28 pp. August, 1959. H.M.S.O., 4s 6d.

6. NEWCOMB, W.A. Hydromagnetic stability of a diffuse linear pinch. Annals of Physics, vol.10, no.2, pp.232-267, June, 1960.

7. SUYDAM, B.R. Stability of a linear pinch. Second International Conference on the Peaceful Uses of Atomic Energy, Geneva, 1958. Proceedings, vol.31, pp.157-159. (Paper 354.)

8. AITKEN, K.L. and others. Pinch stability : theory and experiment. I.A.E.A. Conference on Plasma Physics, Salzburg, September, 1961. (Paper 68.)

9. CHEW, G.F. and others. The Boltzmann equation and the one-fluid hydromagnetic equations in the absence of particle collisions. Proc. Roy. Soc., series A, vol. 236, no.1204, pp.112-118, July, 1956.

10. CHANDRASEKHAR, S. and others. Properties of an ionized gas of low density in a magnetic field. Annals of Physics, vol.2, no.5, pp.435-470, November, 1957, and vol.5, no.1, pp.1-25, September, 1958.

11. STRINGER, T.E. and STOCKER, P.M. Electrostatic instabilities in current-carrying and counter-streaming plasmas and studies of the non-linear Boltzmann-Vlasov equation. I.A.E.A. Conference on Plasma Physics, Salzburg, September, 1961. (Paper 53.)

12. BIRDSALL, D.H., COLGATE, S.A. and FURTH, H.P. The hard-core pinch. Fourth International Conference on Ionization Phenomena in Gases, Uppsala, August, 1959. Proceedings, vol.2, pp.888-895.

13. AITKEN, K.L. and others. Experiments with linear pinch and inverse pinch systems. Fourth International Conference on Ionization Phenomena in Gases, Uppsala, August, 1959. Proceedings, vol.2, pp.896-900.

14. BURKHARDT, L.C. and LOVBERG, R.H. Field configurations and stability in a linear discharge. Second International Conference on the Peaceful Uses of Atomic Energy, Geneva, 1958. Proceedings, vol.32, pp.29-33. (Paper 2395.)

15. SPITZER, L. Physics of fully ionized gases. Interscience, 1956.

16. ADLAM, J.H. and TAYLER, R.J. The diffusion of magnetic fields in a cylindrical conductor. A.E.R.E. T/M 160. 22pp. April, 1958.

17. BICKERTON, R.J. Unpublished.

18. LEES, D.J. et al. Skin formation and diffusion in a toroidal discharge. I.A.E.A. Conference on Plasma Physics, Salzburg, September, 1961. (Paper 52.)

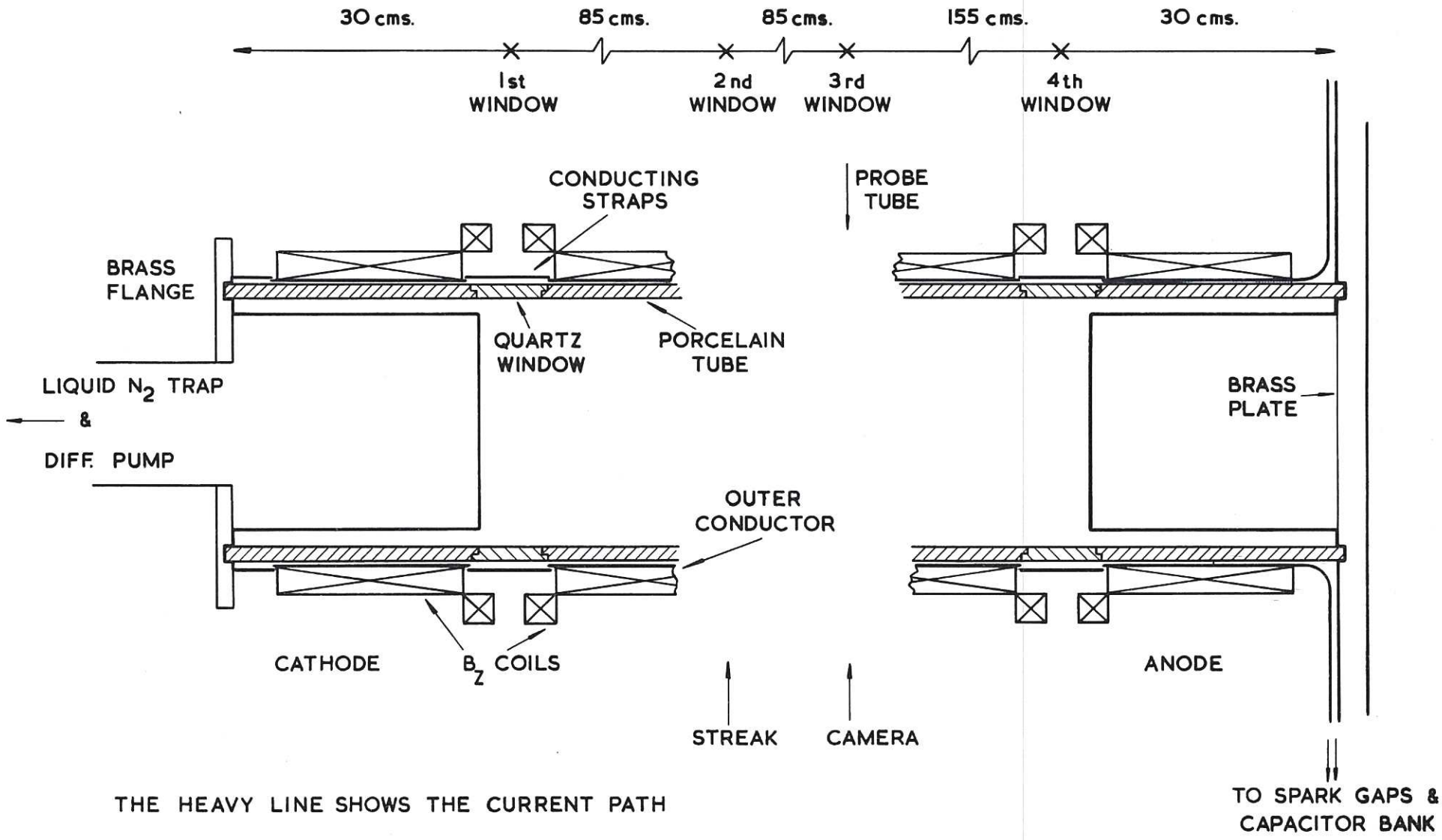

CLM-R 28 Fig. 1 The discharge tube.

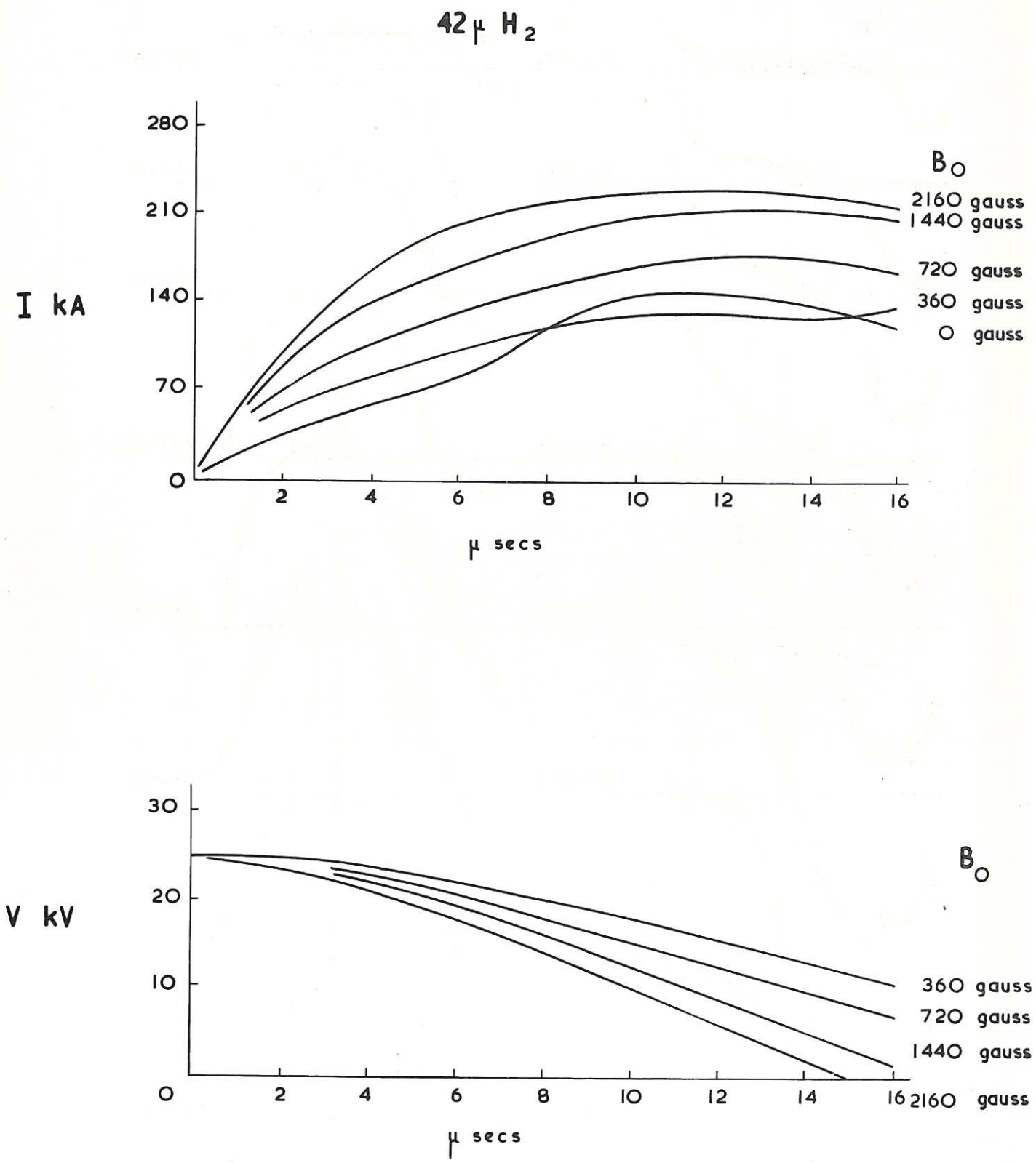

CLM-R 28 Fig. 2 Voltage and current waveforms with different magnetic fields. Gas H_2 at 42 μ Hg.

CLM-R 28 Fig. 3 B_θ and B_z vs radius. (Initial field to be added to B_z) The results were obtained with a multiple probe taking 3 shots for B_θ and 3 for B_z. The vertical lines show the maximum and minimum values.

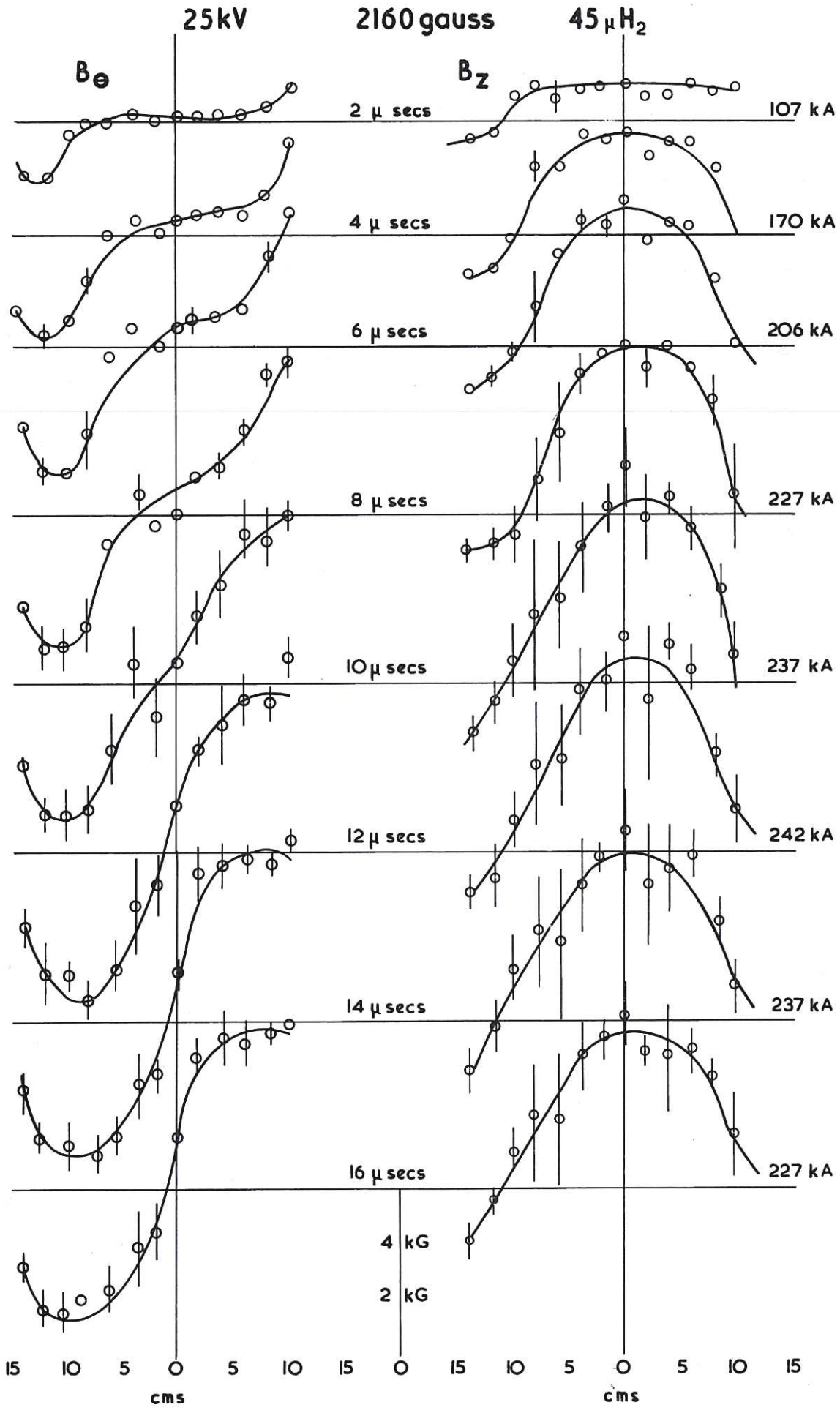

(a) 25 kV, 45 μ H_2, 2160 gauss.

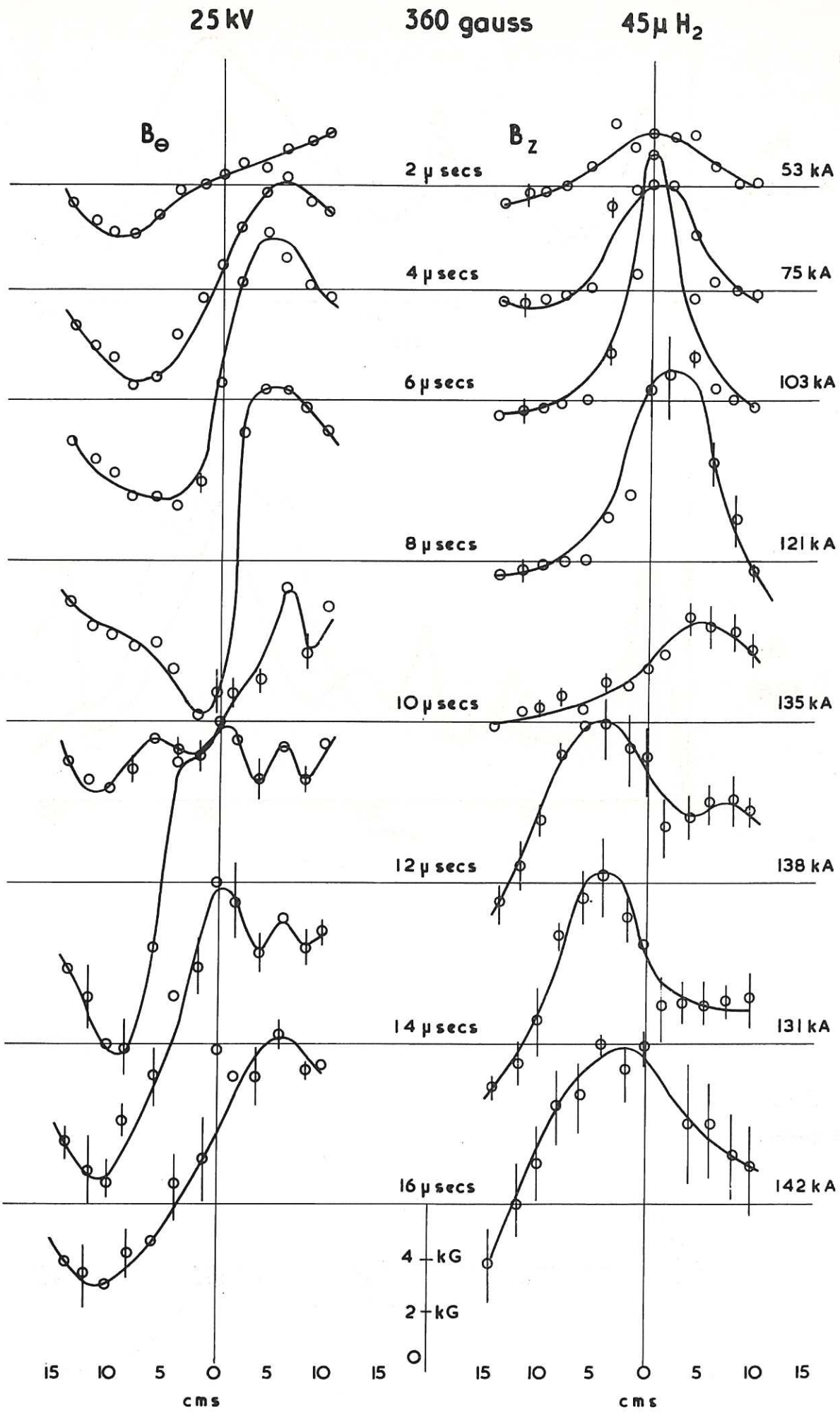

(b) 25 kV, 45 μ H_2, 360 gauss.

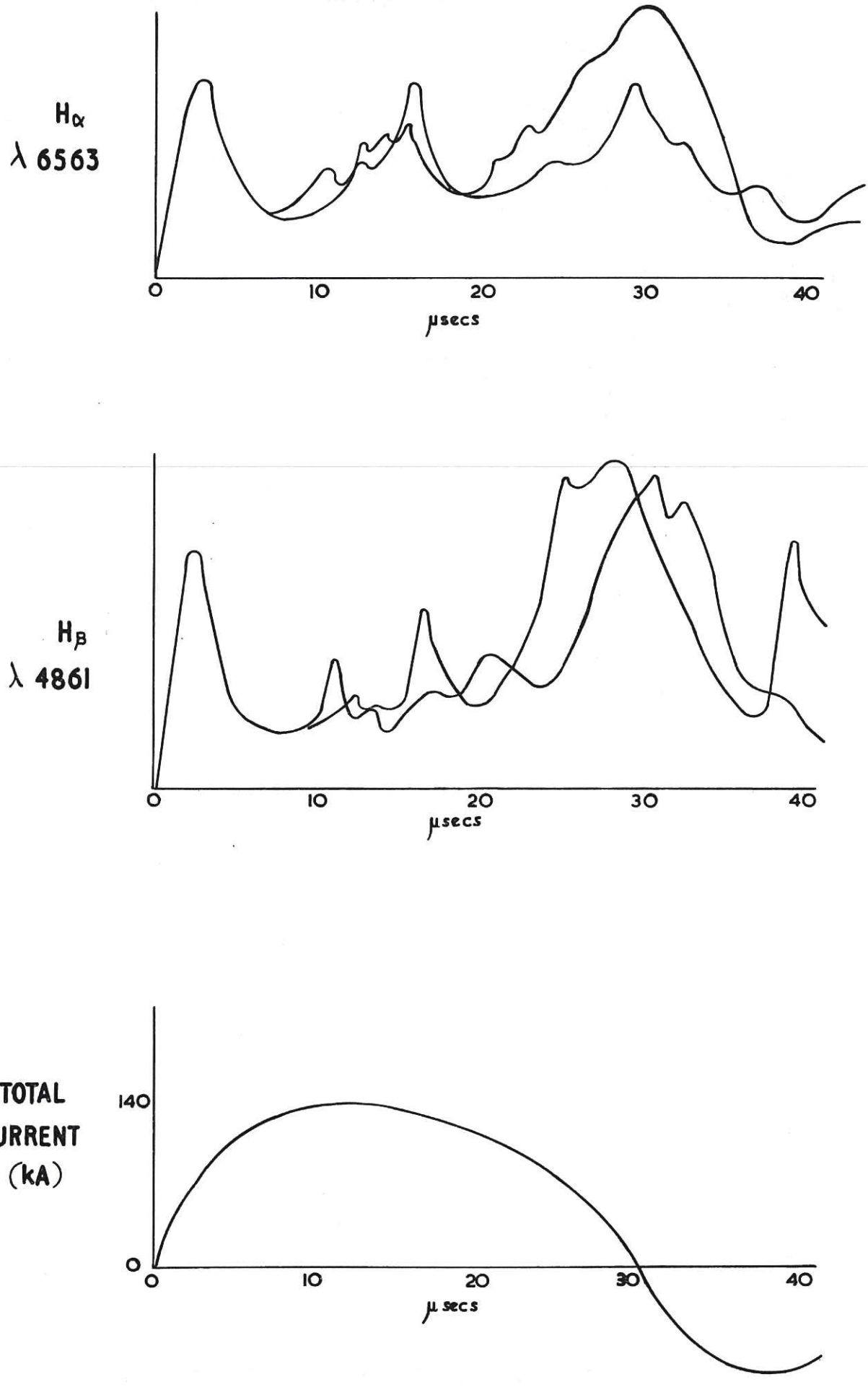

CLM-R 28 Fig. 4 Variation of H_α and H_β intensities 18 kV, 40 μ H_2, 720 gauss.

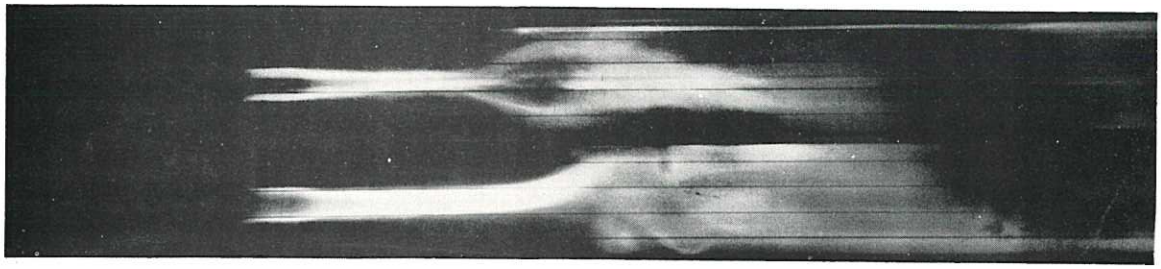

(a) 18 kV, 42 μ H_2, 360 gauss, .44 cms/μ sec.

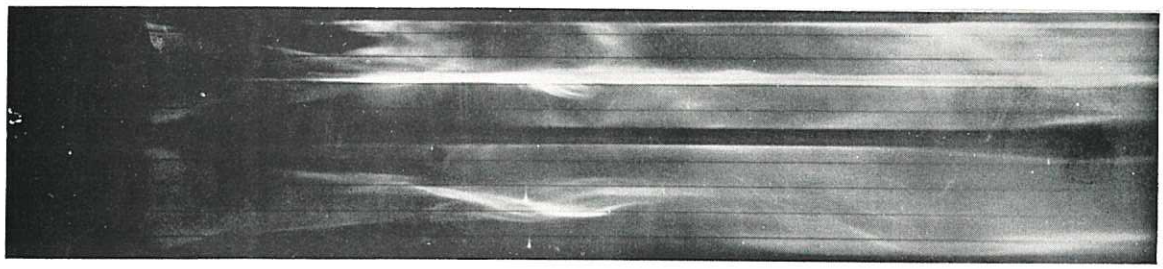

(b) 18 kV, 42 μ H_2, 1440 gauss, .43 cms/μ sec.

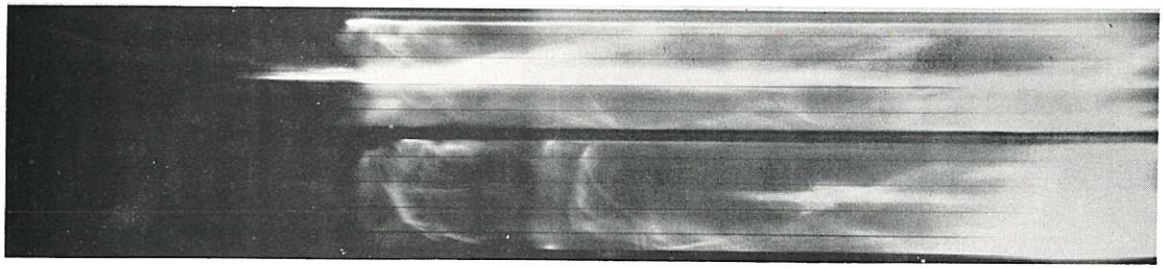

(c) 25 kV, 22 μ H_2, 720 gauss, .40 cms/μ sec.

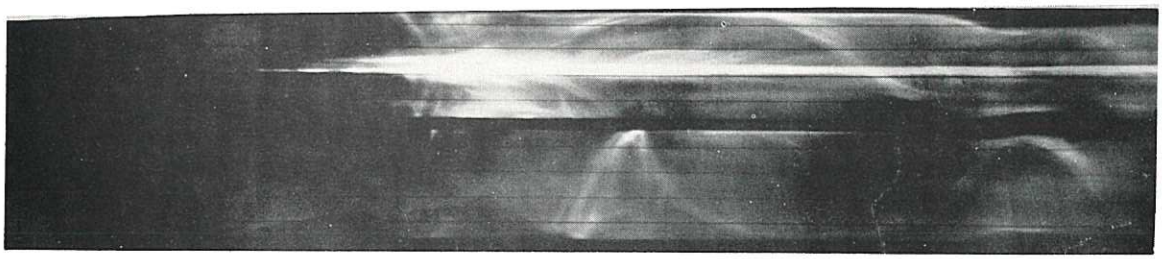

(d) 25 kV, 22 μ H_2, 2160 gauss, .40 cms/μ sec.

CLM-R 28 Fig. 5 The effect of the probe tube on the streak picture under different conditions. The upper picture is the one with the probe tube in each case. Vertical scale - 30 cms (tube diameter) = 2.1 cms.

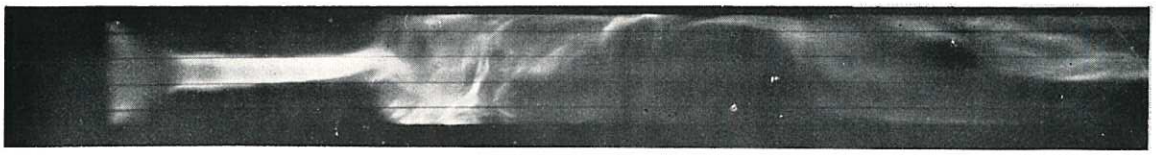

(a) 25 kV, 40 μ H_2, 360 gauss, .40 cms/μ sec.

(b) 25 kV, 44 μ H_2, 720 gauss, .46 cms/μ sec.

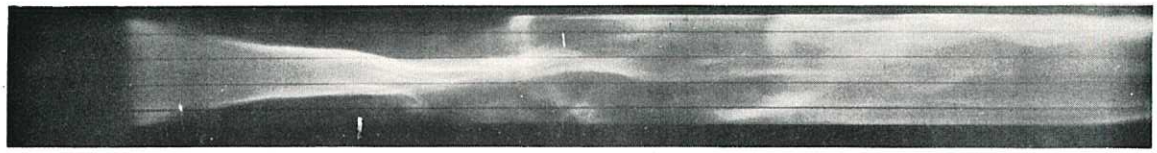

(c) 25 kV, 44 μ H_2, 1440 gauss, .48 cms/μ sec.

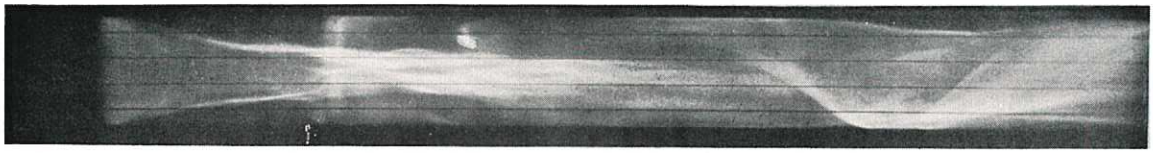

(d) 25 kV, 44 μ H_2, 2160 gauss, .40 cms/μ sec.

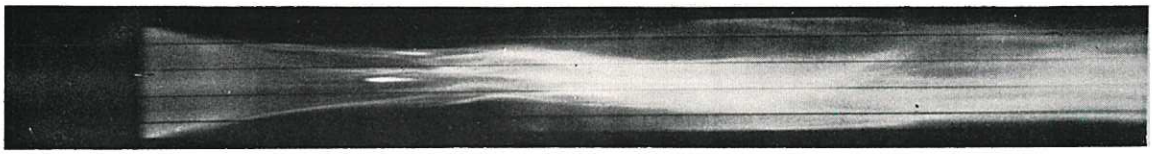

(e) 18 kV, 200 μ H_2, 1440 gauss, .40 cms/μ sec.

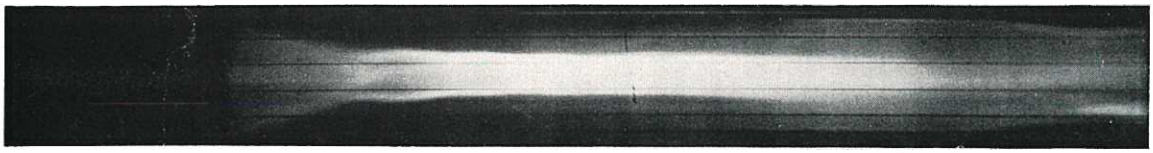

(f) 18 kV, 84 μ He, 720 gauss, .38 cms/μ sec.

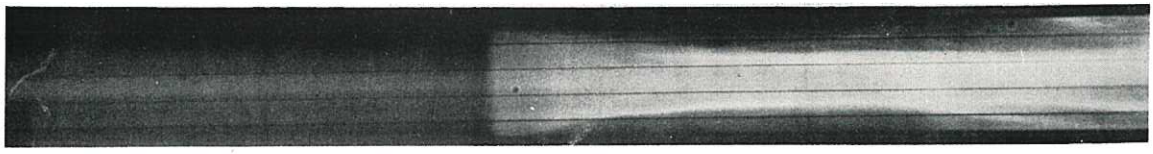

(g) 18 kV, 84 μ He, 1440 gauss, .41 cms/μ sec.

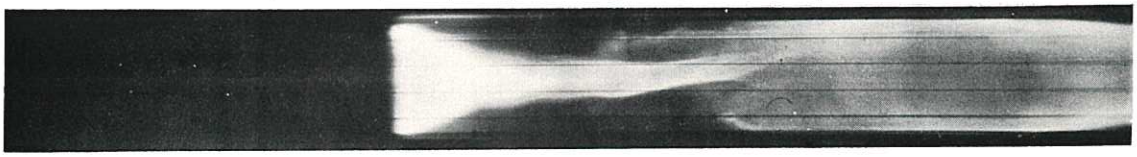

(h) 18 kV, 4 μ A , 720 gauss, .32 cms/μ sec.

CLM-R 28 Fig. 6 Streak pictures under different conditions (no probe tube). Vertical scale - 30 cms (tube diameter) = 2.1 cms.

CLM-R 28 Fig. 7 (a - j) The discharge radius R vs $\frac{\mu I}{2\pi a B_0}$. The numbers on the curves show the time in microseconds. The dotted curves are theoretical for k = 1, and k = 0.5.

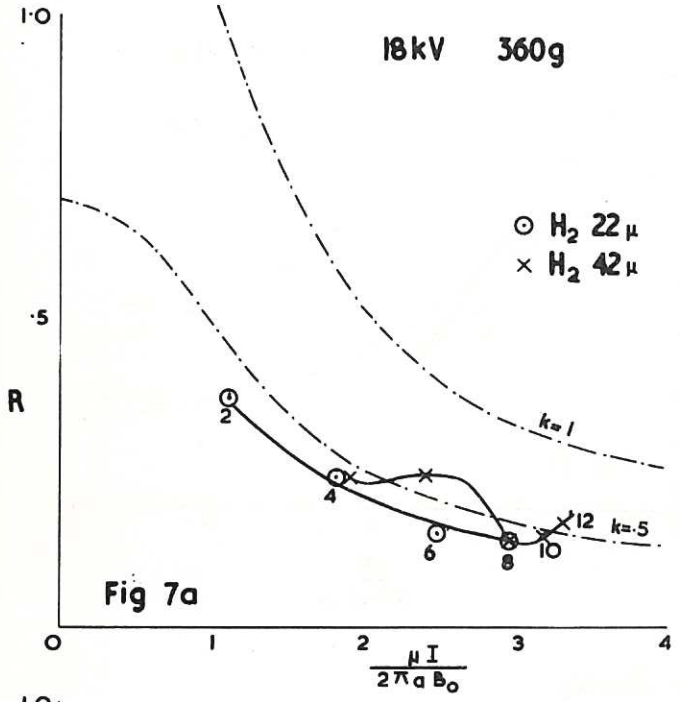

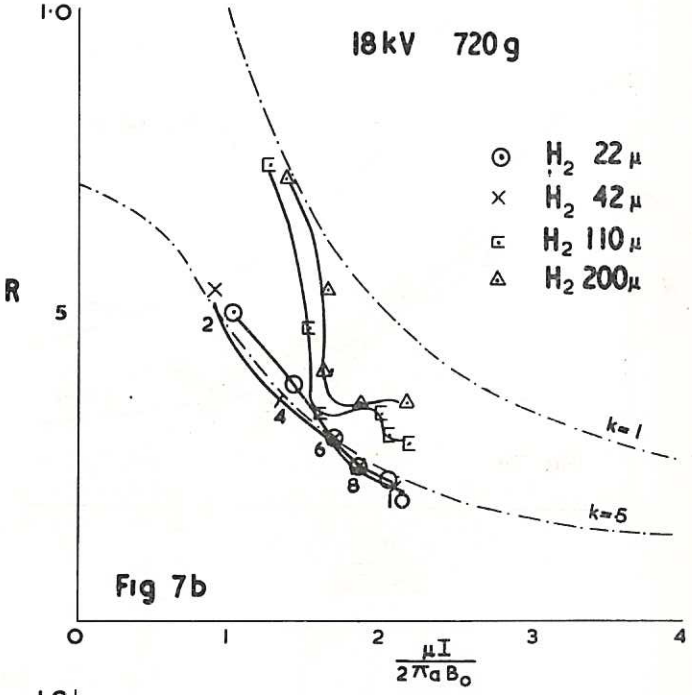

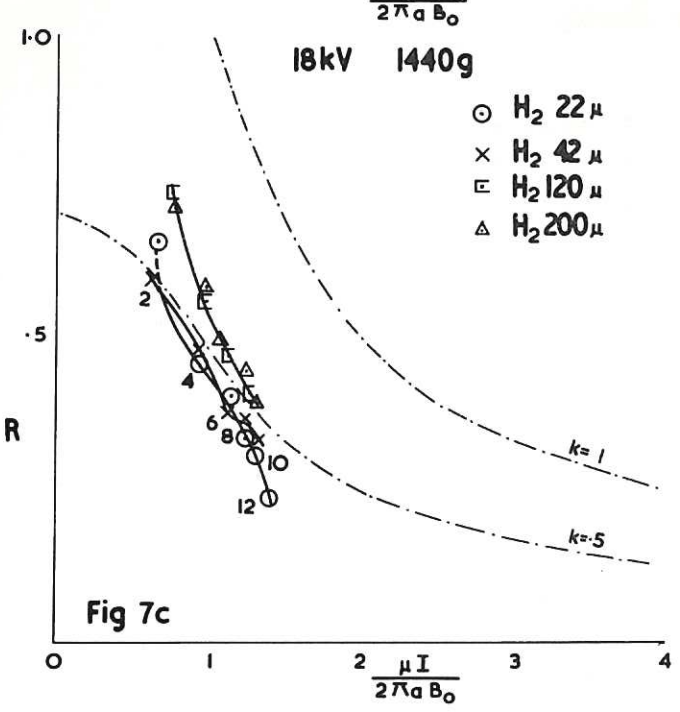

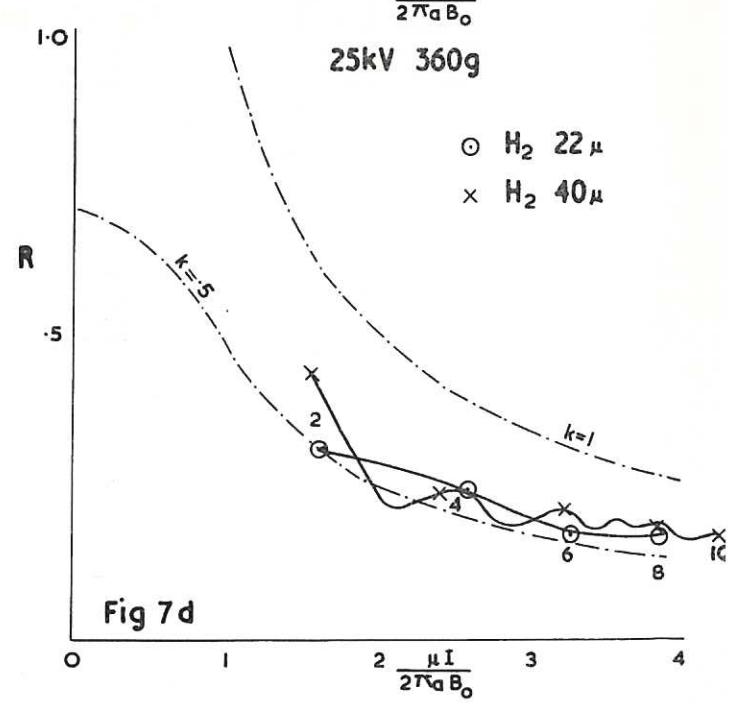

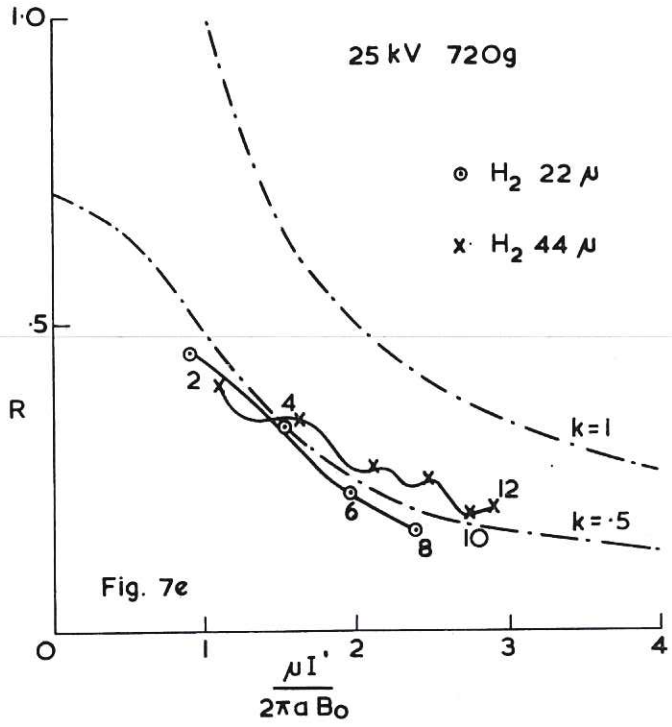

Fig. 7e

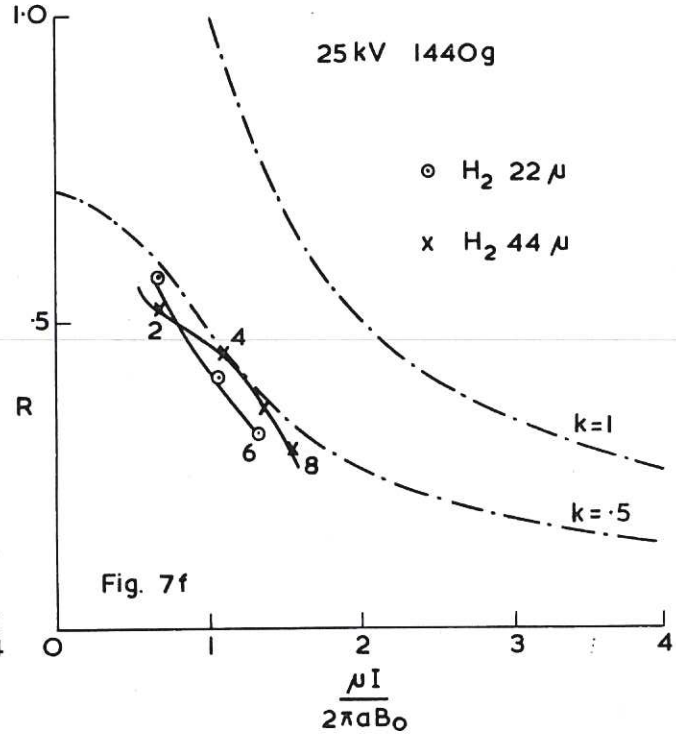

Fig. 7f

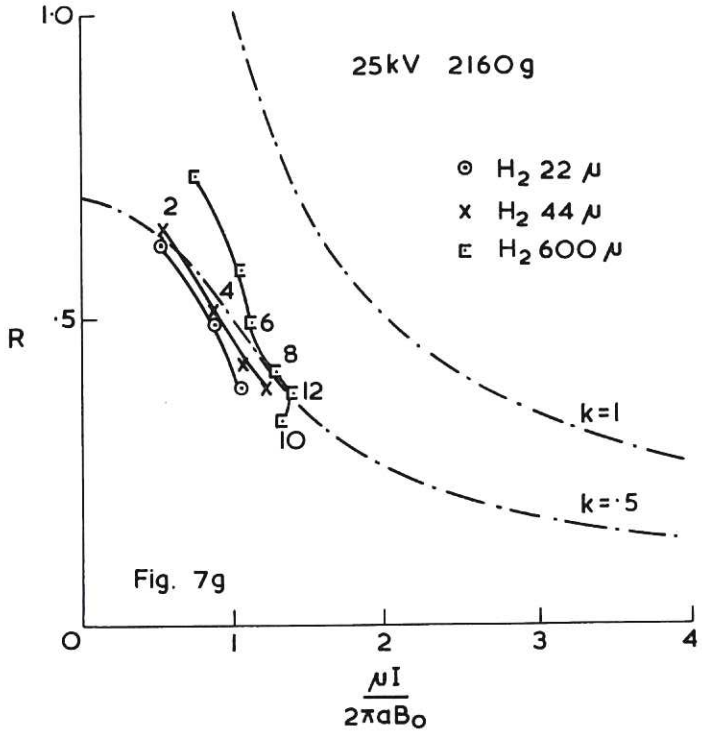

Fig. 7g

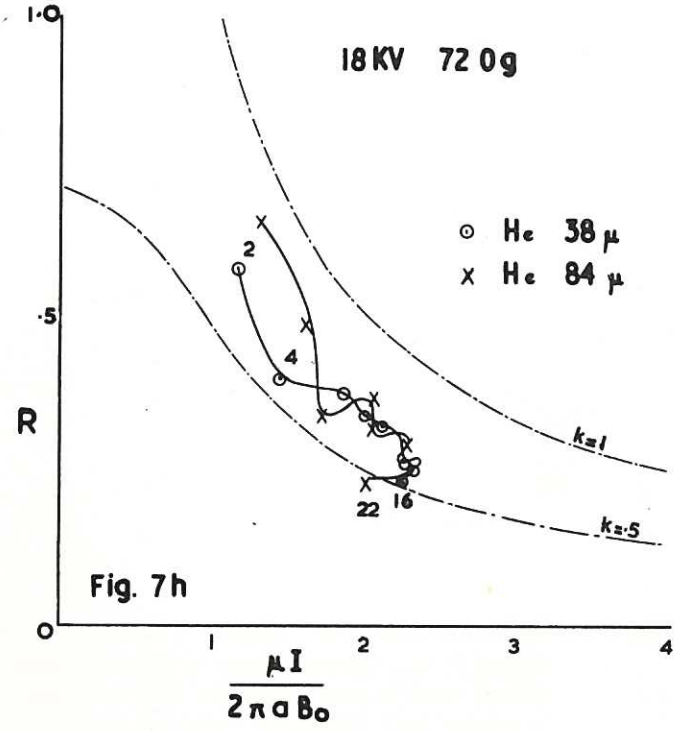

Fig. 7h

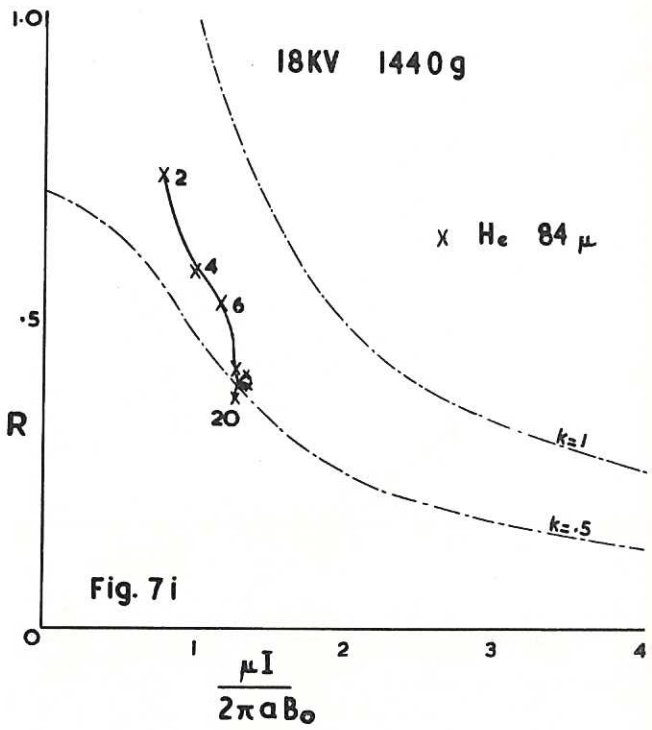

Fig. 7i

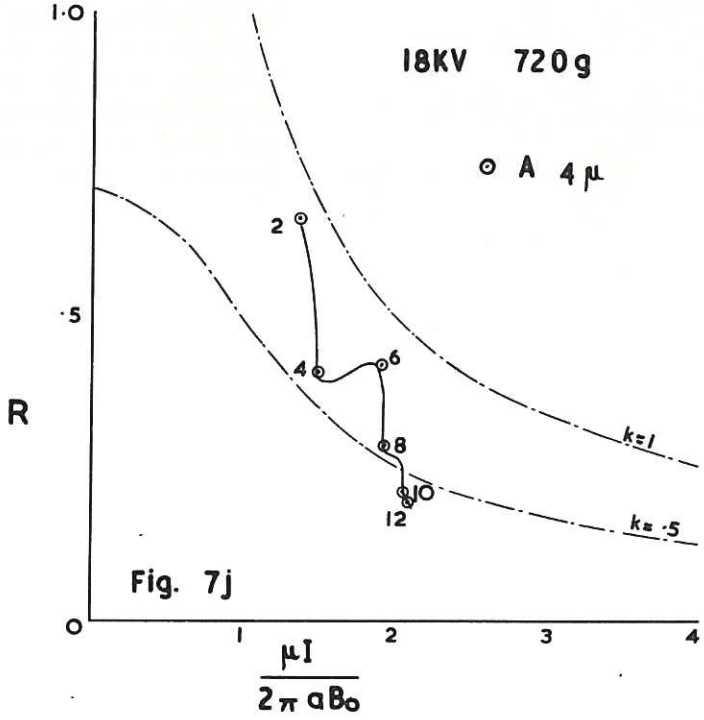

Fig. 7j

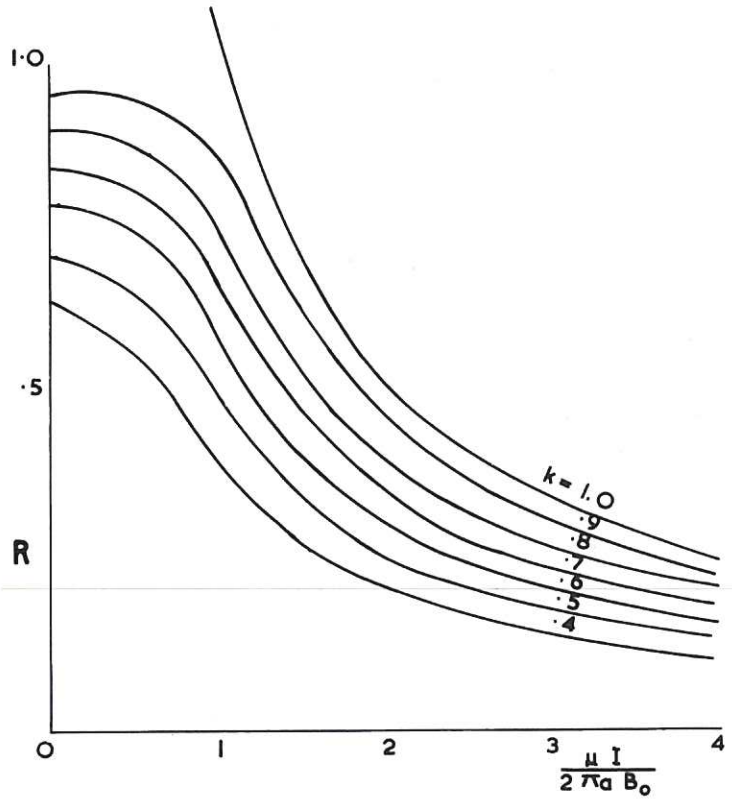

Fig. 8 Theoretical R vs $\frac{\mu I}{2\pi a B_0}$ with $k = \frac{\phi_i}{\phi_0}$

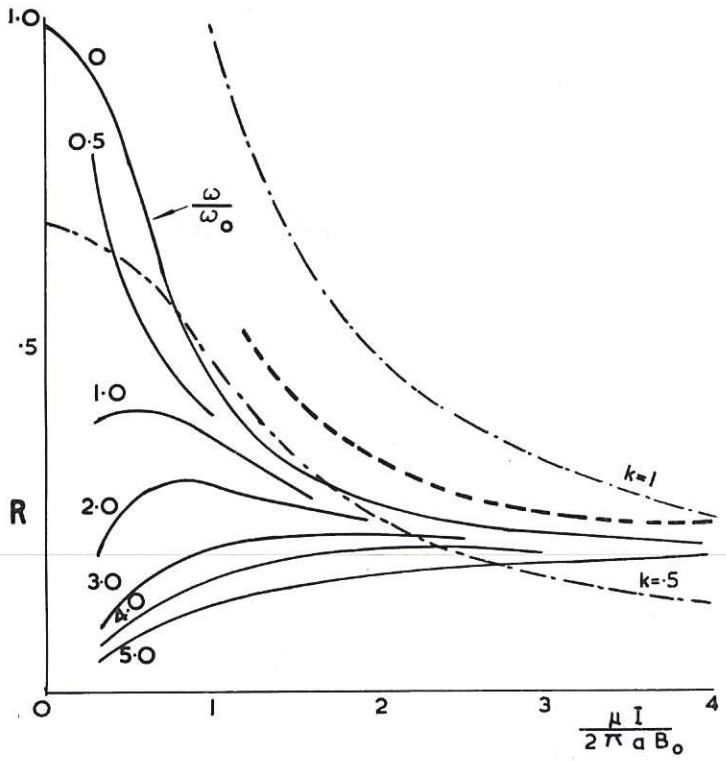

Fig. 9 The maximum instability growth rate ω, normalised to ω_0, the reciprocal of the time for an Alfven wave to cross the tube. Above the line $\omega = 0$ the configuration is 'grossly' stable. Above the heavy dotted line only short wavelength ($kr \to 1/b_e$) surface instabilities are possible. Above the line $k = 1$ (reversed external field) the configuration is stable. (Some generalisation of the theory is necessary before applying to reversed fields in detail).

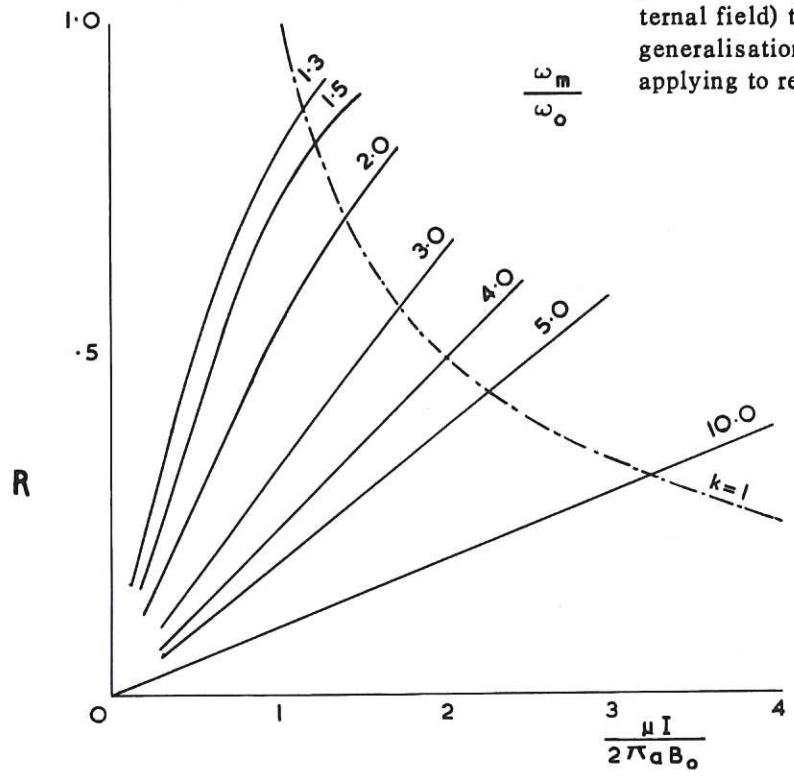

CLM-R 28 Fig.10 The reciprocal of the time for an Alfven wave to cross the discharge, normalised to ω_0. ω_m is always greater than ω_0.

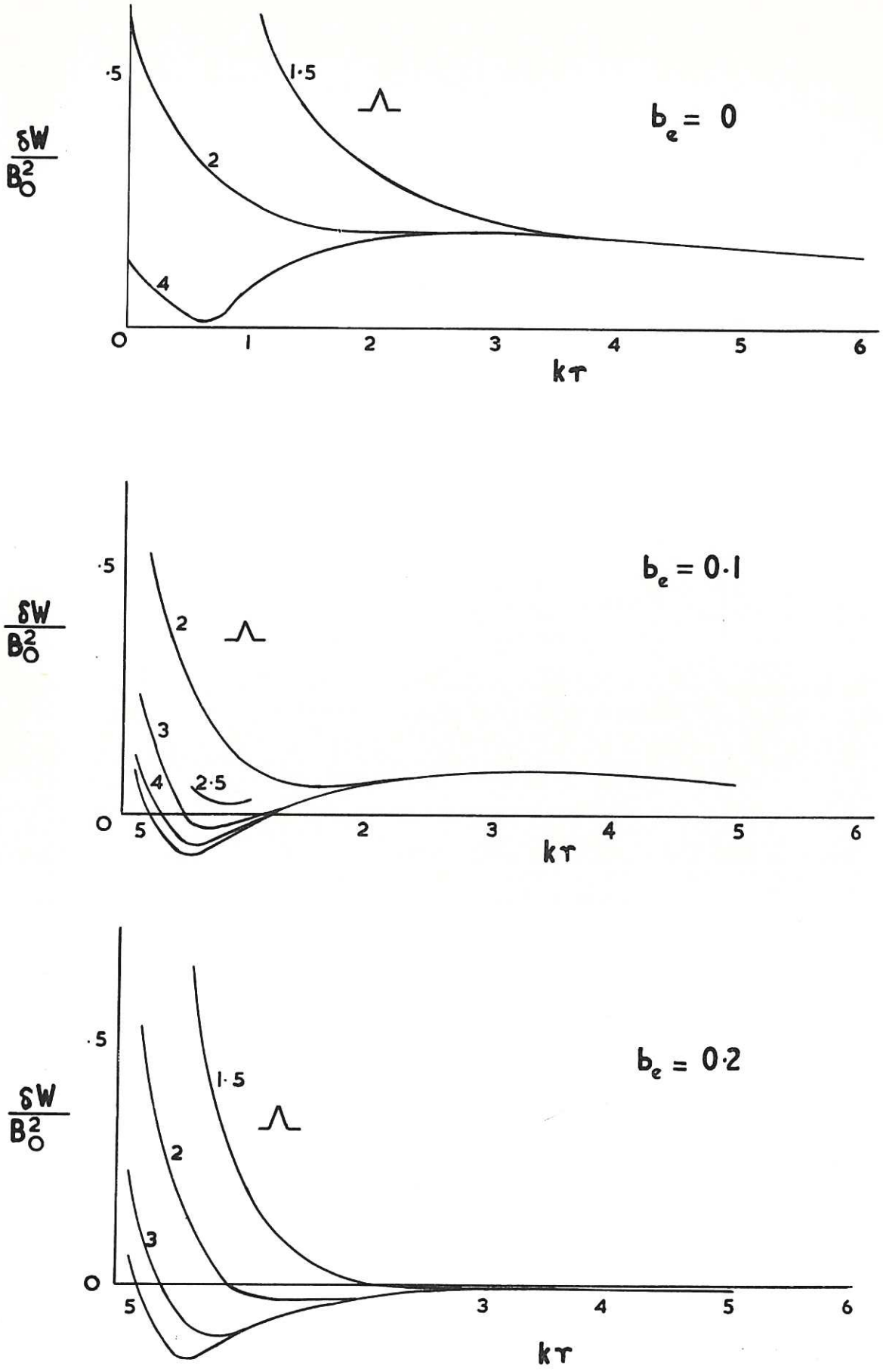

CLM-R 28 Fig.11 δ W vs kr for surface instability with different values of Λ (outer conductor/discharge radius) and b_e (normalised external B_z)

δ W negative indicates surface instability. With b_e + ve δ W is always negative for kr slightly less than $1/b_e$.

Available from

HER MAJESTY'S STATIONERY OFFICE

York House, Kingsway, London W.C. 2

423 Oxford Street, London W. 1

13a Castle Street, Edinburgh 2

109 St. Mary Street, Cardiff

39 King Street, Manchester 2

50 Fairfax Street, Bristol 1

35 Smallbrook, Ringway, Birmingham 5

80 Chichester Street, Belfast

or through any bookseller.

Printed in England

S.O. Code No. 91 - 3 - 14 - 23